5G/mm-Wave Fully-Passive Dual Rotman Lens-Based Harmonic mmID for Long Range Microlocalization Over Wide Angular Ranges

Charles Lynch[ID], *Student Member, IEEE*, Ajibayo O. Adeyeye[ID], *Member, IEEE*,
Aline Eid[ID], *Member, IEEE*, Jimmy G. D. Hester[ID], *Member, IEEE*, and Manos M. Tentzeris[ID], *Fellow, IEEE*

Abstract—In this work, for the first time, a 5G/mm-Wave harmonic frequency modulated continuous wave (FMCW) radar with dual Rotman lens-based harmonic millimeter identification (mmID) ranging system is proposed enabling ultralong range highly accurate localization for future localized sensing cyberphysical systems (CPSs). A detailed characterization of the fully-passive harmonic mmID is first presented with an estimated maximum harmonic radar cross section (RCS) of -35.8 dBsm and a 10 dB beamwidth of $\pm 50°$. The mmID fully overcomes the high-gain beamwidth tradeoff seen in typical high-gain designs enabling robust, ultralong-range detectability. A link budget analysis of the proposed harmonic mmID is presented with the current proof-of-concept (PoC) harmonic radar and with an equivalent isotropic radiated power (EIRP) of 75 dBm reading ranges in excess of 8 km are envisioned. In addition, the system provides a highly accurate ranging at long range with a bounded maximum ranging error of 17 cm up to 46 m from the radar. Furthermore, the 5G/mm-Wave system capitalizes on the highly sensitive phase information for ultrafine 0.4 mm accurate ranging at 10 m. Thus, the proposed system presents a fully-passive, long-range ranging system for future CPSs.

Index Terms—Cyberphysical systems (CPSs), 5G, frequency modulated continuous wave (FMCW), harmonic millimeter identification (mmID), mm-Wave.

I. INTRODUCTION

WITH the recent advances in wireless cyberphysical systems (CPSs) and 5G/mm-Wave technologies, there is a promise of supporting over 75 billion devices on these networks by 2025. As the number of devices scales, an expected proportional number of batteries would be needed and continually replaced in order for these future wireless infrastructures to operate. Thereby, increasing both the maintenance and environmental costs of these CPS and limiting their advancement. In addition, the devices need to be scalable in order

to meet the demand and accuracy of the specific application of these wireless CPS. Given these criteria, a highly favorable form of wireless communication is backscatter through utilizing either radio frequency identification (RFID) or millimeter identification (mmID). These devices do not need to generate their own wireless signal as they encode their sensing information on the interrogating signal and reflect this back to a reader to be processed in the CPS. This form of wireless communication is extremely energy efficient as it eliminates the need for power-hungry components such as a local oscillator (LO) or power amplifier to communicate back to the reader. In addition, due to their minimalist designs, these wireless devices become highly scalable as well. Thus, RFIDs and mmIDs provide an excellent choice to meet the demand of the next-generation wireless CPS. These RFID/mmIDs feature different architectures, namely semi-passive, chipless, and harmonic with each having its own benefits and tradeoffs in cost, encoding information, and operational range. Semi-passive tags provide the longest reading range and can encode the most information back to the reader, however, they are the most expensive to manufacture and require some form of external power supply either from the environment or from the reader [1], [2], [3], [4]. If a semi-passive tag operates through harvesting the transmitting signal their reading range is limited by the reader to mmID link budget. Otherwise, the semi-passive tags are limited in applications where there is environmental energy that can be harvested. Chipless implementations offer the cheapest option and require no external power source, but are limited in reading range due to the static clutter of the environment and the phase-noise of the reader [5], [6], [7]. Harmonic mmIDs provide a highly affordable and fully-passive solution while maintaining sufficient encoding complexity for sensing and tracking applications [8], [9], [10], [11], [12], [13]. These harmonic-based mmIDs rely on receiving a reader signal operating at f_o and backscattering an integer multiple signal operating at nf_o back to the reader which has a receiving channel at nf_o. Due to the harmonic nature of the interrogation, the static clutter in the environment and phase noise which typically masks chipless RFID/mmIDs response are removed, leaving only the harmonic mmID in the receive band. Thus, enabling ultralong range detectability of these harmonic mmIDs. Typically, these harmonic RFID/mmIDs operate in
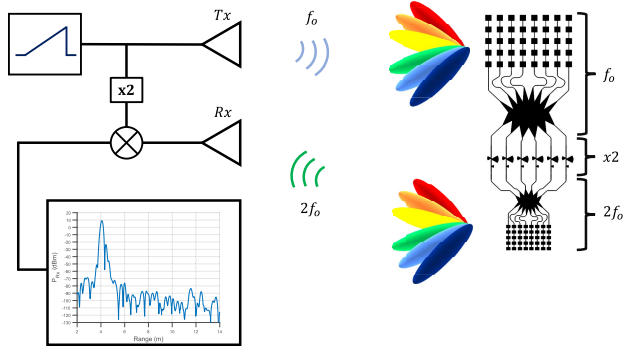
Fig. 1.   Schematic of the proposed harmonic FMCW radar dual Rotman lens-based mmID high-fidelity ranging system.

the ultrahigh-frequency (UHF) or sub-6 GHz bands. From a localization perspective, these lower frequency harmonic tags suffer from a lower bandwidth resource resulting in a lower fidelity ranging on the order of centimeters as well as lower reading distances due to the lower equivalent isotropic radiated power (EIRP). This is crucial for fully-passive harmonic mmIDs as the efficiency of harmonic generation is proportional to the power received at the mmID and therefore, proportional to the transmitting power of the reader. Thus, by shifting up to 5G/mm-Wave operation of the harmonic mmID, one gains additional bandwidth and higher EIRP both regulated by the Federal Communications Commission (FCC) and can achieve both high fidelity localization and long reading ranges. This high-fidelity localization is another important metric for CPS as this allows for the complete and accurate mapping of a physical system to a cyberphysical model that can be utilized for smart city and smart home applications. In [14], Hansen et al. demonstrate some capabilities of this interrogation scheme with a $60/121$ GHz harmonic frequency modulated continuous wave (FMCW) ranging system. However, the harmonic tag utilized was an active harmonic tag requiring a power source at the mmID. In addition, the mmID was not retro-directive and therefore is limited in the maximum reading range of 23 m directly at boresight to the mmID. In [15], Lynch et al. presented a retro-directive dual Rotman lens-based harmonic mmID enabling fully-passive long-range interrogation up to 65 m. In this effort, the authors expand on this work through a complete characterization of this proposed mmID and additionally highlight the high-fidelity ranging capabilities enabled through FMCW radar interrogation and 5G/mm-Wave operation of the device for localized sensing applications in next-generation CPSs. A schematic of this highly accurate localization system is displayed in Fig. 1. The remainder of this article is structured as follows. Section II describes the components of the fully-passive dual Rotman lens-based harmonic mmID. Having characterized the dual Rotman lens-based harmonic mmID, Section III describes the theoretical analysis of the full link budget model for harmonic FMCW radar interrogation. Section IV presents a proof-of-concept (PoC) 14/28 GHz harmonic FMCW radar assembled using off-the-shelf components with an evaluation of both accurate long-range localization and high-fidelity sub-cm microlocalization at 10 m. Finally, Section V concludes with highlights of the presented high-fidelity ranging system while

proposing a framework for multitag and localized sensing applications in next-generation CPSs.

II. 5G/MM-WAVE DUAL ROTMAN LENS-BASED HARMONIC MMID

The dual Rotman lens-based harmonic mmID is made up of two sub-components namely, two harmonic Rotman lenses with their associated eight 5×1 series-fed patch antenna arrays operating at f_o, the transmitting frequency of the reader, and $2 * f_o$, the receiving frequency of the reader, and a miniaturized frequency doubler circuit to generate the harmonic backscattered signal. The architecture for the dual Rotman lens consisted of six beam ports and eight array ports which provides the best tradeoff between angular coverage and array factor gain from the lens, enabling a maximum angular coverage of $\pm 60°$ [16]. By combining the passive beam forming network (BFN) and doubler circuits, the fully-passive mmID enables ultralong-range, wide angular coverage as well as microlocalization of the mmID for 5G-enabled smart city and structural health monitoring CPSs.

A. Evaluation of Dual Rotman Lens-Based Arrays

In order to overcome the high gain, the angular tradeoff in antenna design, two passive BFNs operating at f_o and $2 f_o$, respectively, were designed, fabricated on 0.168 mm thick Rogers 4350 B substrate ($\epsilon_r = 3.55$, $\tan \delta = 0.027$), and are displayed with dimensions in Fig. 2. The radiation properties of the lens-based array at each beam port were characterized by individually exciting each beam port with all other ports terminated with a 50 Ω load to ensure proper operation of the lens. The 14 GHz Rotman lens array was interrogated with a 12 dBi broadband horn antenna and the 28 GHz Rotman lens array was interrogated with a 18 dBi broadband horn antenna. Each Rotman lens-based array was measured at 1 m inside an anechoic environment and rotated $\pm 90°$ in precise steps of $2.5°$ with the angle-dependent gain results of the 14 and 28 GHz Rotman lens arrays displayed in Figs. 3 and 4, respectively.

The peak gain of the 14 and 28 GHz design are 17 and 15 dBi, respectively. In addition, the results display good angular alignment with each corresponding beam port of the two Rotman lens-based arrays being within $2.5°$ of each other for maximum gain on the received 14 GHz signal and retransmission of the 28 GHz signal back to the harmonic radar. The two designs provide a 3 dB beamwdith of $\pm 50°$. Thus, by combining the two harmonic Rotman lens-based arrays, the desired retro-directive behavior is achieved and provides a wide-angular coverage while maintaining high gain for proper backscattering to the harmonic FMCW radar enabling both long-range and high-fidelity ranging.

B. Fully-Passive Miniaturized Frequency Doubler

As previously characterized in [15], a miniaturized frequency doubler operating at the frequencies of the harmonic Rotman lenses and designed on the same Rogers 4350 B substrate was chosen for the generation of the harmonic backscattered response of the mmID back to the reader.
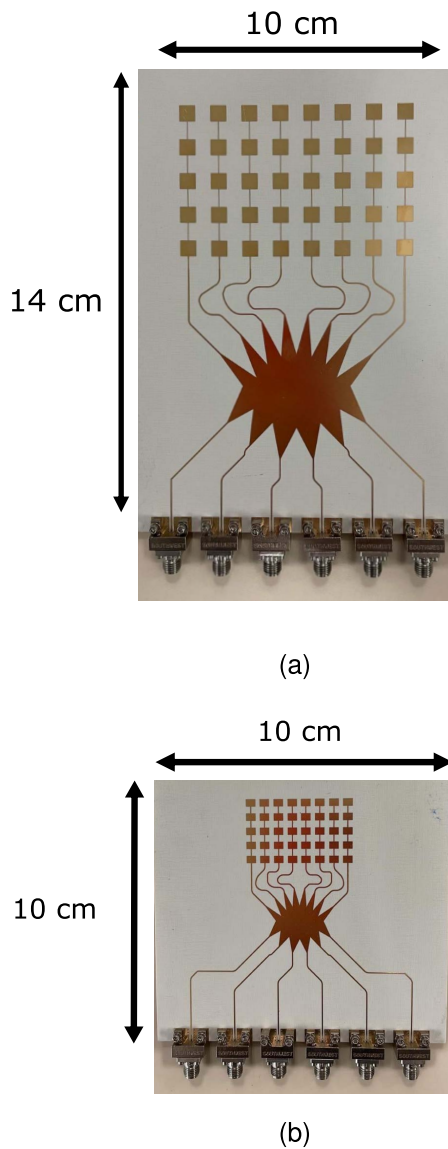
(a)

(b)

Fig. 2.   (a) Fabricated 14 GHz Rotman lens-based array for characterization with 15×10 cm^2 footprint. (b) Fabricated 28 GHz Rotman lens-based array with 7×7 cm^2 footprint.

The fully-passive frequency doubler circuit is comprised of the SMS201, flip-chip, Schottky diode from Macom, due to its high sensitivity resulting in better conversion loss (CL), or more efficient passive harmonic generation. The matching network consists of a single parallel radial stub, and a parallel open circuit radial stub operating at f_o at the input to the diode, to ensure maximum input power into the diode, and finally a short circuit parallel stub operating at f_o to block the fundamental frequency component from the output that could significantly degrade the CL. A surface mount 100 nF capacitor is placed at the output of the frequency doubler to ensure that each diode is not connected in parallel at DC. The 10 dB bandwidth of operation of the fully passive frequency doubler was measured to be 250 MHz centered at 13.94 GHz. The CL of the fully passive frequency doubler was characterized and the schematic with dimensions, simulation and measured results, and an 8th-order polynomial fit of the CL are displayed in Fig. 5. As the results display, the CL of
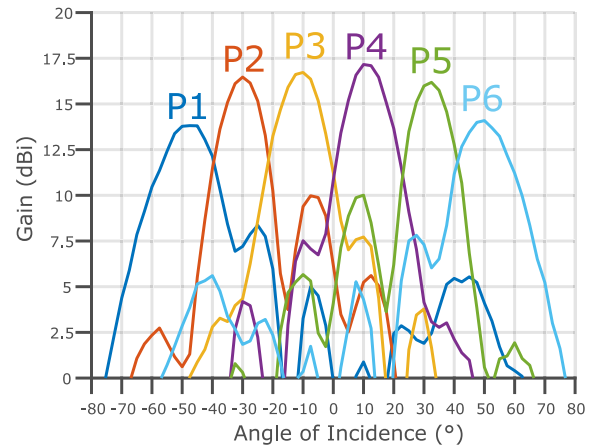

Fig. 3.   Measured angle-dependent gain at 14 GHz for the dual Rotman lens PoC prototype.
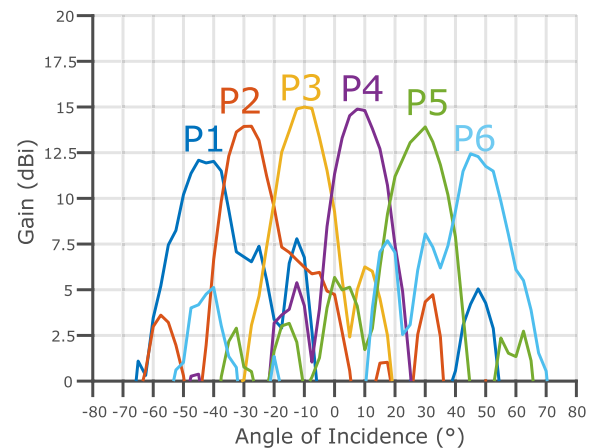
Fig. 4.   Measured angle-dependent gain at 28 GHz for the dual Rotman lens PoC prototype.
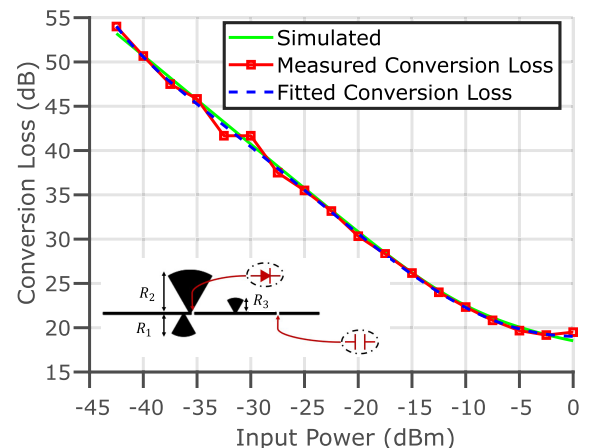
Fig. 5.   Simulated, measured, and 8th order polynomial fit CL along with the circuit layout of the 14/28 GHz frequency doubler with $R_1 = 3.55$ mm, $R_2 = 6.55$ mm, and $R_3 = 2.18$ mm and all radial stubs having an angle of $60°$.

the doubler circuit is adequate for harmonic generation for low input power levels as low as -42.5 dBm, all while requiring no external bias, enabling fully-passive operation at long ranges of the dual Rotman lens-based harmonic mmID.

TABLE I
COMPARISON OF HARMONIC RFID/mmID SYSTEMS WHERE * AND ** DENOTE EIRP'S OF 48 dBm AND 75 dBm, RESPECTIVELY

Ref.	Frequency	EIRP	$\sigma_{RCS_{nf_0}}$	Range
[10]	2.45/4.9 GHz	25 dBm	−57.6 dBsm	5 m
[13]	9.4/18.8 GHz	60.5 dBm	−53.9 dBsm	470 m
[11]	3.5/7 GHz	41.7 dBm	−50.8 dBsm	7 m
[12]	5.9/11.8 GHz	42.1 dBm	−58.4 dBsm	58 m
[14]	61/122 GHz	27 dBm	−41.0 dBsm	23 m
This Work	14/28 GHz	48 dBm	−35.8 dBsm	46*/ 8170 m**

C. Angular Harmonic Radar Cross Section (RCS) of Harmonic Rotman Lens-Based mmID

Having characterized both the angular coverage of each Rotman lens-based array and the performance of the fully-passive miniaturized frequency doubler, the harmonic RCS over the ±90° was calculated using the equation

$$\sigma_{\text{RCS}_{2f_0}} = \frac{G_{f_0} G_{2f_0} \lambda^2_{2f_0} \text{CE}_{@5\text{ m}}}{4\pi} \qquad (1)$$

where G_{f_0}, G_{2f_0}, λ_{2f_0}, and $\text{CE}_{@5\text{ m}}$ are the gain of the 14 GHz Rotman lens-based array in dBi, the gain of the 28 GHz Rotman lens-based array in dBi, the wavelength at the harmonic frequency in meters, and the conversion efficiency which is $1 - \text{CL}_{@5m}$ of the fully-passive doubler at the power level at 5 m from the radar. Using this estimated harmonic RCS versus incidence angle, the mmID presents a peak harmonic RCS of −35.8 dBsm with a 10 dB beamwidth of ±50° and is dislayed in Fig. 6. Thus, highlighting the high detectability over a large angular range of the dual Rotman Lens-based harmonic mmID even in scenarios when the harmonic radar is at an angle of 50° relative to the mmID. In addition, the null at 0° is due to the even number of beam ports on the Rotman lens and can be covered by adding another beam port to the Rotman lens design with the tradeoff being a sacrifice in angular coverage of the harmonic RCS. When compared to other harmonic mmIDs in Table I, the proposed retro-directive harmonic mmID displays a harmonic RCS improvement in excess of 15 dB to other passive harmonic mmIDs and a 5 dB improvement compared to that of an active mmID with a total power consumption of 132 mW. This highlights the superiority of the dual Rotman lens architecture despite requiring no external power source for operation. If the other proposed works were to scale their system in size to increase their detectability—and thus their RCS—the angular coverage would be sacrificed, a problem that was fully overcome in our solution using the dual harmonic Rotman lens. Thus, the proposed fully-passive dual Rotman lens-based harmonic mmID provides a highly detectable response while maintaining a wide angular coverage, thereby improving the robustness of the proposed harmonic FMCW radar mmID ranging system in long-range scenarios.

III. LINK BUDGET ANALYSIS OF HARMONIC FMCW RADAR INTERROGATION

Having characterized the 5G/mm-Wave dual Rotman lens-based harmonic mmID in Section II, now a detailed link
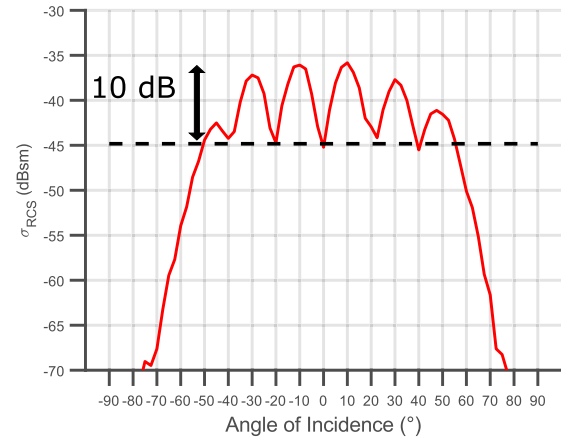

Fig. 6. Estimated angle-dependent harmonic $\sigma_{\text{RCS}_{2f_0}}$ at 5 m from individual fabricated Rotman lens-based arrays gains and CL of doubler with a power level at 5 m.

budget analysis of the device with an ideal reader will be discussed. Four scenarios were considered for analysis. The first two scenarios are with the proposed PoC harmonic radar described in Section IV with an EIRP of 48 dBm with the dual Rotman lens-based harmonic mmID angled at 10° and at 50° highlighting current long-range operation and wide angular coverage of the dual Rotman lens-based architecture. After the same scenario, but with the maximum allowed EIRP of 75 dBm in 5G/mm-Wave bands to demonstrate the benefits to a reading range of harmonic ranging systems. Two propagation paths were considered for this link budget analysis, namely the interrogator to harmonic mmID operating at f_o and the return path operating at in this case the $2f_o$. The power received at the harmonic mmID in dB-scale is described by

$$P_{\text{Rx,tag}} = P_{\text{Tx}} + G_{\text{Tx}} + G_{f_o} + 10n_{f_o} \log_{10}\left(\frac{\lambda_{f_o}}{4\pi R}\right) \qquad (2)$$

where $P_{\text{Rx,tag}}$, P_{Tx}, G_{Tx}, G_{f_o}, n_{f_o}, λ_{f_o}, and R are the power received at the input of the doubler in dBm, the transmitting power of the FMCW radar in dBm, the gain of the transmitting antenna of the radar in dBi, the gain of the mmID fundamental (14 GHz) antenna in dBi, the path loss exponent of the environment at the fundamental frequency of interrogation, the wavelength of the fundamental frequency in meters, and the distance of the mmID from the radar in meters, respectively. Based on the characterization of the fully-passive frequency doubler circuit in Section II-B, the lowest input power that generated a harmonic 28 GHz signal is −42.5 dBm and limiting the maximum operating range of the proposed system by this threshold level. Thus using (2), the received power at the input to the fully passive doubler for all four scenarios is calculated and is displayed in Fig. 7. The plot presents that the harmonic mmID is able to generate the 28 GHz chirp back to the radar up to a range of over 300 and 250 m at the optimal 10° and 50° angle of incidence, respectively. When interrogating with the maximum allowed EIRP of 75 dBm, the harmonic mmID is able to generate the harmonic chirp signal over 10 km away from the harmonic FMCW radar despite an angle of incidence on the mmID of 50°. Therefore, the dual Rotman lens-based architecture supports harmonic generation at ultralong ranges from the
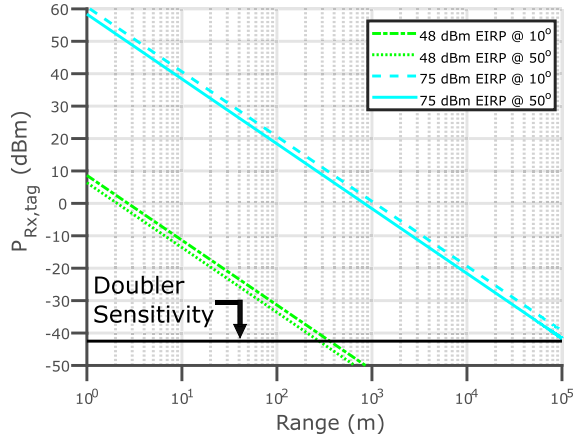
Fig. 7. Received power at the harmonic mmID versus range from the fully-passive dual Rotman lens-based mmID @ angles of incidence of 10° and 50° with $n_{f_o} = n_{2f_o} = 2$.
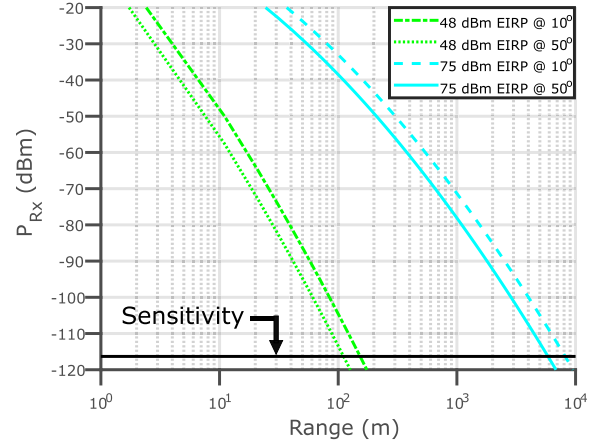

Fig. 8. Received power at the harmonic radar versus range from the fully-passive dual Rotman lens-based mmID @ angles of incidence of 10° and 50° relative to the PoC harmonic radar with $n_{f_o} = n_{2f_o} = 2$.

radar while maintaining wide-angular coverage. After the calculation of the received power at the input of the doubler circuit of the fully-passive harmonic mmID, the incoming FMCW chirp signal is doubled in frequency and retransmitted to the radar. The received power backscattered by the harmonic mmID in dB-scale is described by

$$P_{\text{Rx,Reader}} = G_{\text{Rx}} + \text{CE}\left(P_{\text{Rx,tag}}\right)$$
$$+ G_{2f_o} + 10n_{2f_o} \log_{10}\left(\frac{\lambda_{2f_o}}{4\pi R}\right) \quad (3)$$

where $P_{\text{Rx,Reader}}$, G_{Rx}, $CE(P_{\text{Rx,tag}})$, G_{2f_o}, n_{2f_o}, λ_{2f_o}, are the power received at the reader in dBm, the gain of the receiving antenna of the radar in dBi, conversion efficiency which is a function of the power received by the harmonic mmID in dB, the gain of the mmID harmonic (28 GHz) antenna in dBi, the path loss exponent of the environment at the harmonic frequency, and the wavelength of the harmonic frequency in meters, respectively. The conversion efficiency term for the theoretical link budget analysis is calculated from the negated 8th order polynomial fit of CL of the fully-passive frequency doubler circuit in Section II-B. To estimate the sensitivity level of an ideal reader, chirp periodicity, low-noise amplifier (LNA) gain, and noise figure of the first element was assumed to be 200 kHz, 84.5 ms, 43 dB, and 4 dB corresponding to the proposed PoC harmonic FMCW radar detailed in Section IV. By assuming that the system samples every chirp, the effective sampling rate is then 11.7 Hz and the sensitivity of the reader in dB-scale is described by

$$S_{\text{Rx}} = -174 + G_{\text{LNA}} + \text{NF} + 10\log_{10}\left(F_{\text{Samp}}\right) \quad (4)$$

where G_{LNA}, NF, and F_{Samp} are the gain of the LNA in dBm, noise figure of the LNA in dBm, and effective sample rate in Hz. Thus resulting in a sensitivity of -116.3 dBm. Using (2)–(4), an estimation of the maximum reading range of the PoC harmonic FMCW radar system was calculated with the current EIRP of 48 dBm and the maximum allowable EIRP of 75 dBm in 5G/mm-Waveband. Furthermore, through using the characterized gain of each Rotman lens-based array in Section II-A, the maximum range of the current PoC system and the same system with 75 dBm with the harmonic mmID at

an angle of 50° relative to the harmonic radar was calculated to give the theoretical minimum reading range within the operational beamwidth of the Rotman lens in Fig. 8. The model displays that the current PoC maximum reading range is approximately 150 and 100 m with the angles of incidences impinging on the harmonic mmID of 10° and 50°, respectively. However, by utilizing an allowed EIRP of 75 dBm, the reading range can be extended to over 8 km at an angle of incidence of 10°, an order of magnitude higher than the system proposed in [13]. Further highlighting the long-reading range enabled through the 5G/mm-Wave frequency bands and the superiority of the dual Rotman lens architecture proposed. Even when interrogated at an angle of incidence of 50° relative to the mmID, the minimum reading range is calculated to be over 5 km, enabling long-range detectability over a wide angular coverage. This is due to the fact that the sensitivity level is only constrained by the thermal noise and not the self-interference of the transmitting signal or masked by larger scatterers in the radar's field-of-view (Fov) seen in the typical co-polarized FMCW radar receivers. Thus, through utilizing the proposed retro-directive mmID in combination with the harmonic FMCW radar, fully-passive, ultralong range detectability and high fidelity ranging is enabled for next-generation CPS.

IV. POC 14/28 GHZ HARMONIC FMCW RADAR INTERROGATION

A PoC FMCW radar was assembled to evaluate both the long-range and microlocalization capabilities of the dual Rotman lens-based harmonic mmID. The assembled harmonic FMCW radar can be broken up into the transmitter and receiver chains and a schematic of the assembled harmonic FMCW radar is shown in Fig. 9 with each component of the radar labeled. The transmitter chain of the FMCW radar consists of a 836640L signal generator which produces the FMCW signal which can be expressed in the time domain as

$$s_{\text{Tx}}(t) = A \cos\left(2\pi\left(f_c t + \frac{B}{T_c}t^2\right) + \phi_o\right) \quad (5)$$

where A, f_c, B, T_c, and ϕ_o are the amplitude in V, the carrier frequency of the transmitted signal in Hz, the bandwidth of the
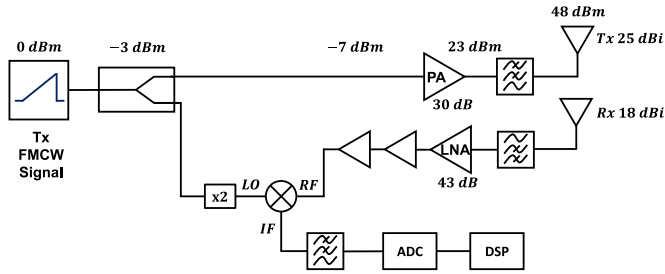
Fig. 9. Block diagram of transmitter and receiver chains of the PoC harmonic FMCW.

FMCW chirp signal in Hz, the chirp periodicity in s, and the initial phase of transmitted waveform in radians, respectively. This signal then passes to a ZC2PD02263-S+ power divider to split the FMCW signal into the transmitting or receiving chain. For the remainder of the transmitting chain, this power-divided FMCW signal passes to a 30 dBm power amplifier to amplify the transmitting signal for long-range interrogation. The signal then passes through an FLP1800 low-pass filter to filter out any harmonics generated by the power amplifier. Afterward, the 14 GHz FMCW signal is transmitted by a 25 dBi standard gain horn antenna to the mmID in the Fov of the radar. The transmitted signal then travels to the fully-passive harmonic mmID where a 28 GHz FMCW signal is generated and focalized back to the PoC harmonic FMCW radar. The mmID signal is then received by a 18 dBi horn antenna in the form of a delayed and frequency-doubled FMCW signal. The signal then passes through a FH1800 high-pass filter to filter out any coupled fundamental frequency signal from the transmitting antenna, and is amplified by a RLNA26G40GB 43 dB LNA to limit the noise floor (NF) of the receiver. Afterward, the signal passes a LNA-40-1800-4000 and an ALN3325-41-2235 to increase the swing of the received signal and is down-mixed with an ADC2640-1 mixer to produce the baseband intermediate frequency (IF) signal. The LO of the mixer consists of the second part of the power-divided FMCW signal from the signal generator which has passed through a HMC578LC3B a wideband frequency doubler to frequency double the transmitting FMCW radar signal. The output of the mixer passes through a baseband lowpass filter to isolate the range spectrum from any high-frequency components that are produced by the mixer. Due to the nature of FMCW waveform, mixing the backscattered doubled and delayed version of the transmitted signal with the frequency-doubled transmitted signal leads to a single frequency tone whose frequency is linearly proportional to two times the round-trip delay time. This resulting time-domain signal is then passed to an oscilloscope for sampling and the IF signal over a single chirp period is expressed by

$$s_{\text{Rx}}(t) = \alpha \cos\left(2\pi\left(2\frac{B}{T_c}\left(\frac{2R}{c}\right)t\right) + \phi_N\right) \qquad (6)$$

where α is the amplitude of the mmID response in V, R is the range of the mmID in meters, c is the speed of light, and ϕ_N is the phase due to the two-way propagation at the lowest frequency of the FMCW slope. The chirp parameters of the PoC 14/28 GHz harmonic radar are displayed in Table II. These parameters dictate the limitations of the

TABLE II
CHIRP PARAMETERS PoC HARMONIC RADAR

Parameter	Value
Fundamental Frequency Range	13.69-14.19 GHz
Harmonic Frequency Range	27.38-28.38 GHz
Bandwidth	500 MHz
Slope	$50\,\text{MHz}\,\text{ms}^{-1}$
Sampling Rate	200 kHz
Chirp Periodicity	85.4 ms
Duty Cycle	11.6%

Fig. 10. Harmonic FMCW radar interrogation of the dual Rotman lens-based mmID at 46 m.

harmonic FMCW radar with the main considerations being the maximum range which is limited by the IF sampling rate and the range resolution which is governed by the bandwidth of the chirp signal. The received IF signal was then sampled on an oscilloscope and was post-processed in MATLAB for either long-range or micolocalization ranging.

A. Evaluation of Long Ranging Capabilities of System

To evaluate the long-range capabilities of the proposed system, the dual Rotman lens-based harmonic mmID was directly aligned with the reader with the mmID itself angled approximately 10° from boresight to provide the maximum harmonic RCS. The harmonic mmID was then ranged from 4 to 46 m in steps of approximately 2 m with the PoC harmonic radar and mmID at a maximum range of 46 m as shown in Fig. 10. Based on the sweeping bandwidth of the harmonic frequency being 1 GHz, the range resolution of the harmonic FMCW radar is 15 cm. At each range, 100 received IF signals were recorded on the oscilloscope and a fast Fourier transform (FFT) of each received IF signal with an FFT length of 2^{17} was applied. Because the mmID is static, a single-range observation was obtained through a spectral average of five range-FFTs. Therefore, from the recorded 100 range-FFTs, the averaging process resulted in 20 total ranging observations of the harmonic mmID at each step. An example of the one averaged range-FFTs with the dual Rotman lens-based harmonic mmID placed 4 m from the PoC FMCW radar is displayed in Fig. 11. In addition to the range measurements, an environmental measurement to determine the noise profile in the PoC harmonic FMCW radar was taken and a moving average was applied to generate an adaptive threshold over range. Then a subtraction of this adaptive threshold level was applied to the averaged range-FFTs and a simple peak find algorithm was used to finally obtain the frequency-based
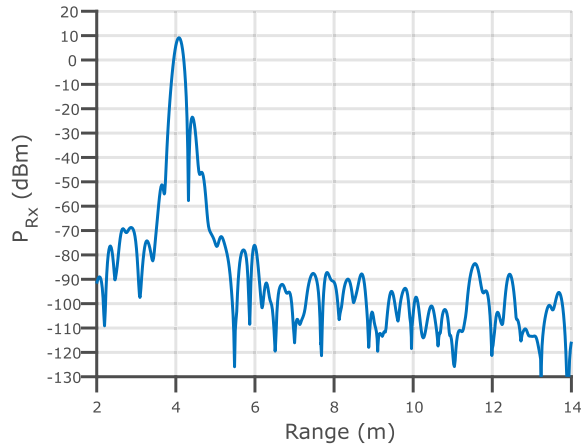
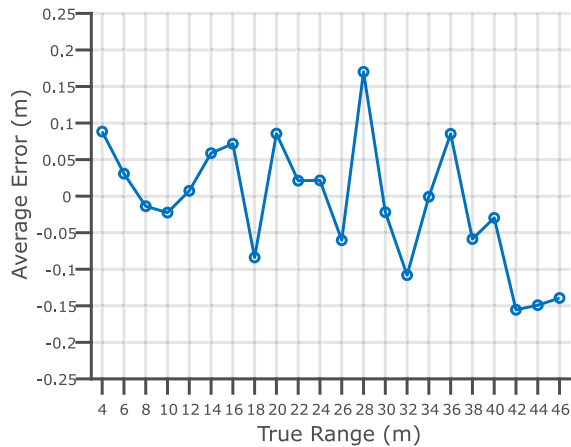Fig. 11. Measured range-FFT spectrum when the harmonic mmID is placed at 4 m from the PoC harmonic FMCW radar.

Fig. 12. Measured average ranging error of proposed fully-passive dual Rotman lens-based harmonic mmID.
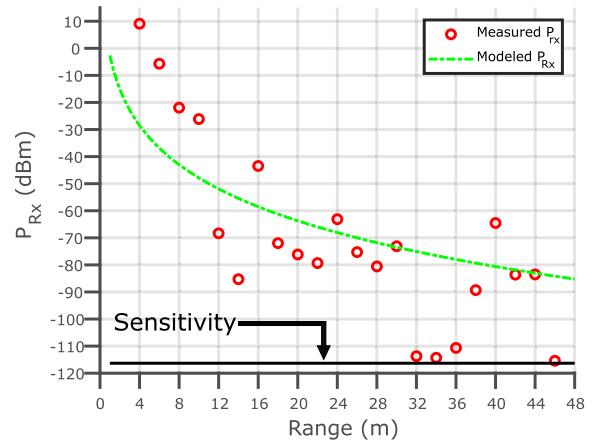

Fig. 13. Measured and theoretical received power of the PoC harmonic FMCW radar versus range of the dual Rotman lens-based harmonic mmID.
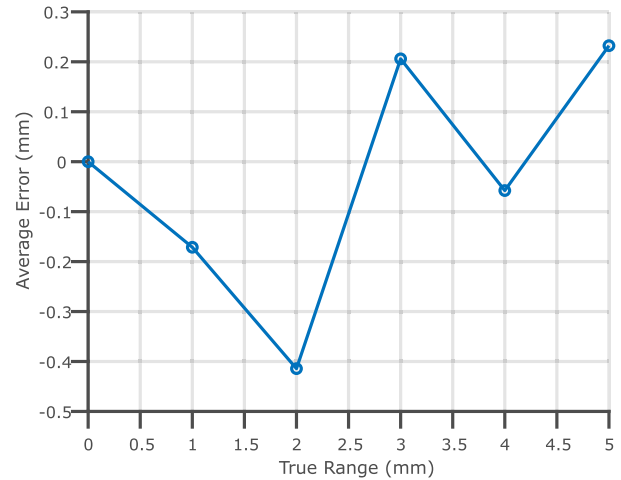

Fig. 14. Measured phase-based average ranging error of harmonic FMCW radar dual Rotman lens-based system.

ranging of the fully-passive harmonic mmID. The ranging error versus the true range is displayed in Fig. 12. With a maximum bounded average error of 17 cm which is within 2 cm of the theoretical range resolution limit of the system, the PoC harmonic FMCW mmID reader displays highly accurate ranging even at long ranges without the need to power the mmID. In addition to the ranging of the fully-passive harmonic mmID, the received power was recorded at each range step and is displayed in Fig. 13. The plot displays good agreement between the theoretical link budget model presented in Section III with some fluctuations with the received power due to the fading in the hallway environment. Thus, the results highlight the long-range detectability of dual Rotman lens-based harmonic mmID while maintaining low average ranging error even at long ranges. Thus, featuring a very good agreement between the measured and modeled received power level as well as a 17 cm ranging accuracy, high accurate ranging at reading ranges of in excess of 8 km utilizing an EIRP of 75 dBm, as mentioned in Section III, is envisioned with the fully-passive dual Rotman lens-based harmonic mmID.

B. Evaluation of Microlocalization of mmID

An evaluation of the microlocalization capabilities of the proposed system was conducted by utilizing the highly sensitive phase information of the IF signal. While phase-based ranging is highly sensitive and can provide fine-scale localization, due to the phase ambiguity every 2π, the ranging information becomes ambiguous without a proper reference to track this phase wrapping. This can be done by utilizing a phase tracking algorithm to resolve these ambiguities and maintain precise ranging information of the desired target. The phase information due to two-way propagation of a harmonic FMCW signal is defined by

$$\phi_N = \frac{2\pi(1+N)R}{\lambda_{f_0}} \quad (7)$$

where ϕ_N, R, N, λ_{f_0} are the phase of the nth harmonic in radians, range of the target in meters, the harmonic multiple, in this case, $N = 2$, and the wavelength of the fundamental frequency, respectively. Due to the mm-Wave operation of the received signal, the wavelength is on the order of cm enabling microlocalization with phased-based ranging. This phase-based ranging was evaluated with the dual Rotman lens-based mmID at 10 nm away from the PoC FMCW radar and the mmID was then precisely stepped on a track from 0 to 5 mm in steps of 1 mm. For the phase estimation, a similar 100 observations of the static harmonic mmID were

recorded on the oscilloscope. Afterward a range-FFT was taken over each IF signal with an FFT of length 2^{19}. The target was detected through the same peak detection over the 100 observations and the phase of the detected peak was recorded. By using the (7) and tracking the change in phase at each step from the initial position, the estimated range of the harmonic mmID was calculated. From these 100 phase-based ranging estimates, an average error from the true displacement was calculated with the results displayed in Fig. 14. The proposed system displayed a bounded average error of 0.41 mm highlighting the system's micro-localization accuracy at stand-off ranges. Thus, the proposed dual Rotman lens-based harmonic mmID presents a unique opportunity for highly accurate microlocalization of wireless sensing applications in next-generation CPSs.

V. CONCLUSION

In conclusion, the author presented a 5G/mm-Wave enabled harmonic FMCW radar fully-passive dual Rotman lens-based ranging system. Thorough characterization of the dual Rotman lens-based harmonic mmID was presented and the proposed retro-directive mmID displayed a peak harmonic RCS of -35.8 dBsm with 10 dB beamwidth of $\pm 50°$. Thus the harmonic mmID presents a high-detectability while maintaining good angular coverage providing for a more robust and ultra-long reading range of the mmID without requiring external power. The dual Rotman lens-based topology maintains superiority in terms of reading range and harmonic RCS even when compared against an active mmID. Using this characterization, a theoretical link budget of the harmonic mmID was presented and with an EIRP of 75 dBm, the model estimates reading ranges in excess of 8 km. The ranging system was evaluated for both ranging accuracy at long ranges with the harmonic mmID ranging system having a maximum average ranging error of 17 cm up to 46 m from the PoC radar. Furthermore, microlocalization of the system was evaluated and presented a maximum average error of 0.4 mm at 10 m from the PoC radar highlighting the system's high fidelity localization capabilities. While the current size of the harmonic mmID is relatively large in size, through utilizing the same dual Rotman lens-based topology and scaling the fundamental frequency up to 29 GHz, a size reduction of approximately 50%. Furthermore, multitag interrogation is supported through frequency division multiplexing of the harmonic mmID which is enabled due to the wide bandwidths at 5G/mm-Wave frequencies. Thereby, the proposed system presents an architecture for fully-passive interrogation at ultralong and with highly accurate localization capabilities for future cyberphyscial systems.

REFERENCES

[1] A. Eid, J. G. D. Hester, and M. M. Tentzeris, "Rotman lens-based wide angular coverage and high-gain semipassive architecture for ultralong range mm-wave RFIDs," *IEEE Antennas Wireless Propag. Lett.*, vol. 19, no. 11, pp. 1943–1947, Nov. 2020.

[2] J. G. Hester and M. M. Tentzeris, "A mm-wave ultra-long-range energy-autonomous printed rfid-enabled Van-Atta wireless sensor: At the crossroads of 5G and IoT," in *IEEE MTT-S Int. Microw. Symp. Dig.*, Jun. 2017, pp. 1557–1560.

[3] S. J. Thomas, E. Wheeler, J. Teizer, and M. S. Reynolds, "Quadrature amplitude modulated backscatter in passive and semipassive UHF RFID systems," *IEEE Trans. Microw. Theory Techn.*, vol. 60, no. 4, pp. 1175–1182, Apr. 2012.

[4] A. Athalye, V. Savic, M. Bolic, and P. M. Djuric, "Novel semi-passive RFID system for indoor localization," *IEEE Sensors J.*, vol. 13, no. 2, pp. 528–537, Feb. 2013.

[5] J. G. D. Hester and M. M. Tentzeris, "Inkjet-printed flexible mm-wave Van-Atta reflectarrays: A solution for ultralong-range dense multitag and multisensing chipless RFID implementations for IoT smart skins," *IEEE Trans. Microw. Theory Techn.*, vol. 64, no. 12, pp. 4763–4773, Dec. 2016.

[6] E. M. Amin, M. S. Bhuiyan, N. C. Karmakar, and B. Winther-Jensen, "Development of a low cost printable chipless RFID humidity sensor," *IEEE Sensors J.*, vol. 14, no. 1, pp. 140–149, Jan. 2014.

[7] D. Girbau, A. Ramos, A. Lazaro, S. Rima, and R. Villarino, "Passive wireless temperature sensor based on time-coded UWB chipless RFID tags," *IEEE Trans. Microw. Theory Techn.*, vol. 60, no. 11, pp. 3623–3632, Nov. 2012.

[8] V. Palazzi, F. Alimenti, P. Mezzanotte, G. Orecchini, and L. Roselli, "Analysis of a multi-node system for crack monitoring based on zero-power wireless harmonic transponders on paper," in *Proc. IEEE Topical Conf. Wireless Sensors Sensor Netw. (WiSNet)*, Jan. 2018, pp. 92–95.

[9] P. Li, Z. An, L. Yang, P. Yang, and Q. Lin, "RFID harmonic for vibration sensing," *IEEE Trans. Mobile Comput.*, vol. 20, no. 4, pp. 1614–1626, Apr. 2021.

[10] V. Palazzi, F. Alimenti, P. Mezzanotte, G. Orecchini, and L. Roselli, "Zero-power, long-range, ultra low-cost harmonic wireless sensors for massively distributed monitoring of cracked walls," in *IEEE MTT-S Int. Microw. Symp. Dig.*, Jun. 2017, pp. 1335–1338.

[11] X. Gu, N. N. Srinaga, L. Guo, S. Hemour, and K. Wu, "Diplexer-based fully passive harmonic transponder for Sub-6-GHz 5G-compatible IoT applications," *IEEE Trans. Microw. Theory Techn.*, vol. 67, no. 5, pp. 1675–1687, May 2018.

[12] D. Psychoudakis, W. Moulder, C.-C. Chen, H. Zhu, and J. L. Volakis, "A portable low-power harmonic radar system and conformal tag for insect tracking," *IEEE Antennas Wireless Propag. Lett.*, vol. 7, pp. 444–447, 2008.

[13] R. Maggiora, M. Saccani, D. Milanesio, and M. Porporato, "An innovative harmonic radar to track flying insects: The case of vespa velutina," *Sci. Rep.*, vol. 9, no. 1, pp. 1–10, Dec. 2019.

[14] S. Hansen, C. Bredendiek, G. Briese, and N. Pohl, "A compact harmonic radar system with active tags at 61/122 GHz ISM band in SiGe BiCMOS for precise localization," *IEEE Trans. Microw. Theory Techn.*, vol. 69, no. 1, pp. 906–915, Jan. 2021.

[15] C. Lynch, A. Adeyeye, A. Eid, J. Hester, and M. M. Tentzeris, "Ultra-long-range dual Rotman lenses-based harmonic mmID's for 5G/mm-wave IoT applications," in *IEEE MTT-S Int. Microw. Symp. Dig.*, Jun. 2022, pp. 32–35.

[16] A. Eid, J. G. D. Hester, and M. M. Tentzeris, "5G as a wireless power grid," *Sci. Rep.*, vol. 11, no. 1, pp. 1–9, Jan. 2021.
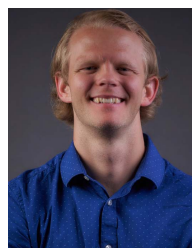
Charles Lynch (Student Member, IEEE) received the B.S. degree in electrical engineering from the Rose-Hulman Institute of Technology, Terre Haute, IN, USA, in 2019. He is currently pursuing the M.S. and Ph.D. degrees in electrical engineering at the Georgia Institute of Technology, Atlanta, GA, USA.

He is a Research Assistant with the ATHENA Group, Georgia Institute of Technology. His current research interests include the design, simulation, and fabrication of RF and millimeter-wave devices, specifically RFIDs and mmIDs and combining these low-power, wearable, ultralow-cost devices with radar for the Internet of Things systems.

Ajibayo O. Adeyeye (Member, IEEE) received the B.S. degree (magna cum laude) in electrical and electronics engineering from the Rose-Hulman Institute of Technology, Terre Haute, IN, USA, in 2017. He is currently pursuing the Ph.D. degree in electrical engineering at the Georgia Institute of Technology, Atlanta, GA, USA.

His research interests lie at the intersection of RADAR and RFID systems for localization applications.

Mr. Adeyeye was awarded First Place in the 2019 IEEE Microwave Theory and Techniques Society International Microwave Symposium Student Design Competition on Backscatter Radio and was the Best Student Paper Finalist at the 2021 International Microwave Symposium.

Aline Eid (Member, IEEE) received the M.S. degree in electrical and computer engineering from the American University of Beirut, Beirut, Lebanon, in 2017, and the Ph.D. degree in electrical and computer engineering from the Georgia Institute of Technology, Atlanta, GA, USA, in Spring 2022.

She is currently a Post-Doctoral Associate at the MIT Media Laboratory, Signal Kinetics Group, Massachusetts Institute of Technology, Cambridge, MA, USA. She will be joining the Department of Electrical Engineering and Computer Science, University of Michigan, Ann Arbor, MI, USA, as an Assistant Professor, in January 2023. In 2020, she did a six-month internship with the Google wearable/augmented reality (AR)/virtual reality (VR) and advanced technology projects (ATAP) groups. She is an inventor of four patents. She has authored or coauthored more than 50 conference papers and journal articles and book chapters. Her research interests are in millimeter wave (mm-wave)-enabled harvesting, backscattering communications and sensing solutions for smart environments and infrastructures.

Dr. Eid was a recipient of the 2020 IEEE MTT-S Graduate Fellowship and Tom Brazil Awards and the First Place Award in the Student Poster Competition at the 2020 FLEX MEMS Sensors Technical Congress. During her master's and Ph.D. studies, she was a recipient of more than 16 awards. At the 2019 IEEE International Microwave Symposium (IMS) conference, she received the First Place in the Radio Frequency Identification (RFID) Student Design Competition, the Second Place and Audience Choice in the 3 MT Competition, and an Honorable Mention in the Student Paper Competition. She received the First Place in the Best Student Paper Award Competition at the 2021 IEEE Antennas and Propagation Society (AP-S).

Jimmy G. D. Hester (Member, IEEE) received the M.S. and Ph.D. degrees in electrical and computer engineering from the Georgia Institute of Technology, Atlanta, GA, USA, in 2014 and 2019, respectively.

He is now a Co-Founder and the CTO at Atheraxon, Atlanta, the company commercializing the 5G RFID technology. His research expertise lies at the interface between radio frequency and mm-wave system engineering, material science, and radar signal processing. He has developed solutions for the use of carbon nanomaterials as well as optimized RF structures toward the implementation of inkjet-printed flexible low-cost ubiquitous gas sensors for the Internet of Things and smart skin applications, along with the hardware and signal processing schemes required for their accurate tracking and wireless powering.

Dr. Hester was awarded the 2015 NT4D Student Award, the 2nd Place Best Poster Award at the 2017 IEEE Futurecar Conference, the 3rd Place Best Poster Award at the 2017 Flex Conference, and the Honorable Mention Award as a Finalist of the 2017 International Microwave Symposium (IMS) Student Paper Competition.

Manos M. Tentzeris (Fellow, IEEE) received the Diploma degree (magna cum laude) in electrical and computer engineering from the National Technical University of Athens, Athens, Greece, and the M.S. and Ph.D. degrees in electrical engineering and computer science from the University of Michigan, Ann Arbor, MI, USA, in 1993 and 1998, respectively.

He was a Visiting Professor with the Technical University of Munich, Munich, Germany, in 2002, with Georgia Tech Research Institute (GTRI)-Ireland, Athlone, Ireland, in 2009, and with

Laboratoire d'analyse et d'architectures des systèmes - Centre National de la Recherche Scientifique (LASS-CNRS), Toulouse, France, in 2010. He is currently a Ken Byers Professor in flexible electronics with the School of Electrical and Computer Engineering, Georgia Institute of Technology, Atlanta, GA, USA, where he heads the ATHENA Research Group (20 researchers). He has served as the Head for the GTECE Electromagnetics Technical Interest Group, as the Georgia Electronic Design Center Associate Director of RFID/Sensors Research, as the Georgia Institute of Technology NSF-Packaging Research Center Associate Director of RF Research, and as the RF Alliance Leader. He has authored more than 850 papers in refereed journals and conference proceedings, seven books, and 26 book chapters. He has helped develop academic programs in 3-D/inkjet-printed RF electronics and modules, flexible electronics, origami and morphing electromagnetics, highly integrated/multilayer packaging for RF, millimeter-wave, sub-THz and wireless applications using ceramic and organic flexible materials, paper-based RFID's and sensors, wireless sensors and biosensors, wearable electronics, "Green" electronics, energy harvesting and wireless power transfer, nanotechnology applications in RF, microwave MEMs, and SOP-integrated (UWB, multiband, mmW, and conformal) antennas.

Dr. Tentzeris is a member of the Union Radio Scientifique Internationale (URSI)-Commission D and the MTT-15 Committee, an Associate Member of European Microwave Association (EuMA), a Fellow of the Electromagnetic Academy, and a Member of the Technical Chamber of Greece. He served as one of the IEEE MTT-S Distinguished Microwave Lecturers from 2010 to 2012 and is one of the IEEE Council on RFID (CRFID) Distinguished Lecturers. He has given more than 100 invited talks to various universities and companies all over the world. He was a recipient/co-recipient of the 2022 Georgia Tech Outstanding Doctoral Thesis Advisor Award, the 2019 Humboldt Research Prize, the 2017 Georgia Institute of Technology Outstanding Achievement in Research Program Development Award, the 2016 Bell Labs Award Competition 3rd Prize, the 2015 IET Microwaves, Antennas, and Propagation Premium Award, the 2014 Georgia Institute of Technology Electrical and Computer Engineering (ECE) Distinguished Faculty Achievement Award, the 2014 IEEE RFID-TA Best Student Paper Award, the 2013 IET Microwaves, Antennas and Propagation Premium Award, the 2012 FiDiPro Award in Finland, the iCMG Architecture Award of Excellence, the 2010 IEEE Antennas and Propagation Society Piergiorgio L. E. Uslenghi Letters Prize Paper Award, the 2011 International Workshop on Structural Health Monitoring Best Student Paper Award, the 2010 Georgia Institute of Technology Senior Faculty Outstanding Undergraduate Research Mentor Award, the 2009 IEEE TRANSACTIONS ON COMPONENTS AND PACKAGING TECHNOLOGIES Best Paper Award, the 2009 E. T. S. Walton Award from the Irish Science Foundation, the 2007 IEEE Antennas and Propagation Society (AP-S) Symposium Best Student Paper Award, the 2007 IEEE MTT-S International Microwave Symposium (IMS) Third Best Student Paper Award, the 2007 International Symposium on Antennas and Propagation (ISAP) 2007 Poster Presentation Award, the 2006 IEEE MTT-S Outstanding Young Engineer Award, the 2006 Asia–Pacific Microwave Conference Award, the 2004 IEEE TRANSACTIONS ON ADVANCED PACKAGING Commendable Paper Award, the 2003 National Aeronautics and Space Administration (NASA) Godfrey "Art" Anzic Collaborative Distinguished Publication Award, the 2003 International Bank of Commerce (IBC) International Educator of the Year Award, the 2003 IEEE Components, Packaging, and Manufacturing Technology (CPMT) Outstanding Young Engineer Award, the 2002 International Conference on Microwave and Millimeter-Wave Technology Best Paper Award (Beijing, China), the 2002 Georgia Institute of Technology–ECE Outstanding Junior Faculty Award, the 2001 Applied Computational Electromagnetics Society (ACES) Conference Best Paper Award, the 2000 NSF CAREER Award, and the 1997 Best Paper Award of the International Hybrid Microelectronics and Packaging Society. He was the Technical Program Chair (TPC) Chair of the IEEE MTT-S IMS 2008 Symposium and the Chair of the 2005 IEEE Computational Electromagnetics in Time-Domain(CEM-TD) Workshop. He is the Vice-Chair of the RF Technical Committee (TC16) of the IEEE CPMT Society. He is the Founder and the Chair of the RFID Technical Committee (TC24) of the IEEE MTT-S and the Secretary/Treasurer of the IEEE Coucil on RFID (C-RFID). He is an Associate Editor of the IEEE TRANSACTIONS ON MICROWAVE THEORY AND TECHNIQUES, the IEEE TRANSACTIONS ON ADVANCED PACKAGING, and the *International Journal of Antennas and Propagation*.